Journal of Biomedical Optics

Dense concentric circle scanning protocol for measuring pulsatile retinal blood flow in rats with Doppler optical coherence tomography

Bingyao Tan
Zohreh Hosseinaee
Kostadinka Bizheva

SPIE.

Dense concentric circle scanning protocol for measuring pulsatile retinal blood flow in rats with Doppler optical coherence tomography

Bingyao Tan,[a] **Zohreh Hosseinaee,**[b] **and Kostadinka Bizheva**[a,b,c,]*

[a]University of Waterloo, Department of Physics and Astronomy, Waterloo, Ontario, Canada
[b]University of Waterloo, Department of System Design Engineering, Waterloo, Ontario, Canada
[c]University of Waterloo, School of Optometry, Waterloo, Ontario, Canada

Abstract. The variability in the spatial orientation of retinal blood vessels near the optic nerve head (ONH) results in imprecision of the measured Doppler angle and therefore the pulsatile blood flow (BF), when those parameters are evaluated using Doppler OCT imaging protocols based on dual-concentric circular scans. Here, we utilized a dense concentric circle scanning protocol and evaluated its precision for measuring pulsatile retinal BF in rats for different numbers of the circular scans. An spectral domain optical coherence tomography (SD-OCT) system operating in the 1060-nm spectral range with image acquisition rate of 47,000 A-scans/s was used to acquire concentric circular scans centered at the rat's ONH, with diameters ranging from 0.8 to 1.0 mm. A custom, automatic blood vessel segmentation algorithm was used to track the spatial orientation of the retinal blood vessels in three dimensions, evaluate the spatially dependent Doppler angle and calculate more accurately the axial BF for each major retinal blood vessel. Metrics such as retinal BF, pulsatility index, and resistance index were evaluated for each and all of the major retinal blood vessels. The performance of the proposed dense concentric circle scanning protocols was compared with that of the dual-circle scanning protocol. Results showed a 3.8 ± 2.2 deg difference in the Doppler angle calculation between the two approaches, which resulted in ~7% difference in the calculated retinal BF. © The Authors. Published by SPIE under a Creative Commons Attribution 3.0 Unported License. Distribution or reproduction of this work in whole or in part requires full attribution of the original publication, including its DOI. [DOI: 10.1117/1.JBO.22.11.110501]

*Address all correspondence to: Kostadinka Bizheva, E-mail: kbizheva@uwaterloo.ca
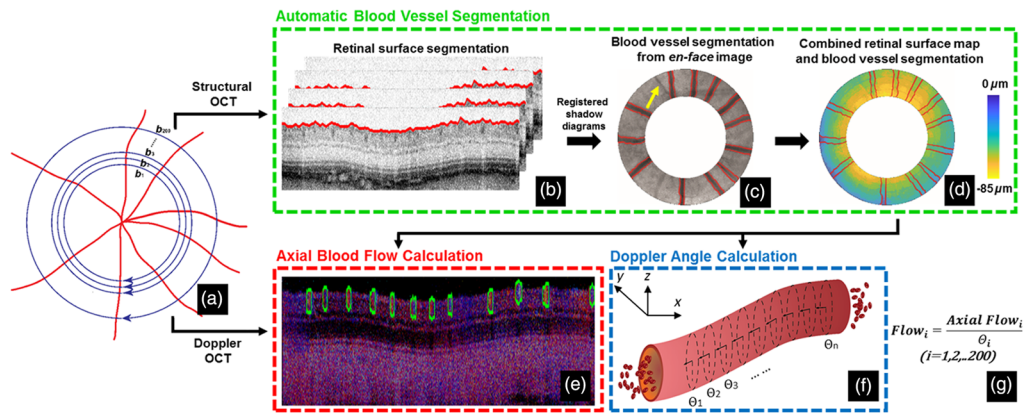
1 Introduction

Pulsatile retinal blood flow (BF) is associated with a number of ocular vascular-related diseases, such as diabetic retinopathy,[1] central retinal venous occlusion,[2] age-related macular degeneration,[3] and glaucoma.[4] Recent studies[1–4] indicated that metrics that characterize the pulsatility of retinal BF are sensitive to early pathophysiological changes in the retina, therefore accurate assessment of retinal BF pulsatility can aid the early diagnosis of potentially blinding diseases. Previously, different optical imaging modalities, such as scanning laser ophthalmology,[5] laser Doppler velocimetry,[6] and retinal vessel analyzer[7] have been used for assessment of the pulsatility of retinal BF. In comparison, Doppler optical coherence tomography (DOCT) offers higher sensitivity and provides simultaneously both structural and BF/blood perfusion information about the imaged object, which offers an opportunity to examine the relationship between morphological and BF changes in the retina induced by retinal diseases.[8] Since DOCT measures only axial BF along the imaging beam direction, precise knowledge of the angle between the incident beam and the blood vessel is necessary in order to assess absolute retinal BF. Dual-beam DOCT[9,10] utilizes two imaging beams incident on the same location in the imaged blood vessel in order to determine more precisely the absolute BF. However, this method requires more complex and expensive design of the OCT system, while precise alignment of the two imaging beams at the same location in the retina can be difficult and time consuming. An alternative approach to measuring absolute retinal BF with DOCT is to utilize a dual-circle scanning pattern[6] and use the location displacement of blood vessels between the two circular OCT scans to calculate the Doppler angle. One limitation of this approach is that it is based on the assumption that the retinal blood vessel runs along a straight line between the two circular OCT scans, which is frequently not the case. A virtual concentric scan[11] method and an OCT angiography-based approach[12] have also been proposed for absolute BF assessment. Both of these methods utilize a raster-scanned volumetric OCT image stack of the retina and repeated circular OCT scans that are acquired separately, and later coregistered with the volumetric images in order to determine the Doppler angle of blood vessels. These approaches are very sensitive to eye motion artifacts, while precise registration of the retinal blood vessels between the circular scans and the volumetric image stacks can be problematic. *En-face* Doppler OCT[13,14] offers a Doppler angle-independent approach to calculation of the absolute retinal BF by integrating the axial BF from an *en-face* image. However, this approach requires ultrafast image acquisition or excellent synchronization of the OCT images with the cardiac cycle.

Here, we present an alternative scanning protocol that utilizes a dense concentric circular scan pattern over a doughnut-shaped area of the retina centered at the optic nerve head (ONH), and an automatic retinal blood vessel segmentation algorithm, for more precise quantification of the absolute and pulsatile retinal BF. This new approach was tested in the rat retina and results were compared with the dual-circle scan approach for absolute retinal BF measurement.

2 Methods

A research-grade, spectral domain OCT system, designed and built by our group for various imaging studies in the animal retina[15–17] was modified for use in this study. Briefly, a broad bandwidth superluminescent diode ($\lambda_c = 1060$ nm, $\Delta\lambda = 110$ nm, Superlum Ltd., Ireland) was used to achieve 3.5-μm

Fig. 1 Flow chart for the absolute retinal BF assessment. (a) Diagram of concentric scans with variable diameter, centered at the ONH. (b–d) Automatic blood vessel segmentation protocol: (b) Retinal surface segmentation for each concentric scan (red line). The area between the two cyan dashed lines is averaged axially to generate a shadow image (c) in which blood vessel are segmented and marked with red lines. The yellow arrow marks a branched blood vessel that is not segmented by the automatic algorithm. (d) A retinal surface elevation map where all segmented blood vessels are marked. (e) A representative DOCT cross sectional image labeled with segmented blood vessels. (f) Diagram for precise Doppler angle calculation of the spatially dependent magnitude and direction of the retinal BF. (g) Formula for calculating the absolute BF from the i'th circular scan.

axial resolution in retinal tissue. The DOCT retinal imaging probe, comprised of three broadband NIR achromat doublet lenses ($f_1 = 10$ mm, $f_2 = 60$ mm, and $f_3 = 30$ mm; Edmund Optics, Barrington, New Jersey) and a pair of galvanometric scanners (Cambridge Technologies, Bedford, Massachusetts), was designed to deliver a collimated imaging beam of 1.5 mm diameter to the rat cornea, thus achieving ~5-μm lateral resolution in retinal tissue. The optical power of the imaging beam at the corneal surface was 1.7 mw, which is below the maximum permissible exposure as per the ANSI guidelines.[18] A high-resolution spectrometer (P&P Optica, Waterloo, Canada) and an NIR line scan camera (1024-LDH2 92 kHz, Sensors Unlimited) were used at the detection end of the DOCT system.

Male Brown Norway rats ($n = 10$) weighting ~300 g were used in this study to test the new DOCT scanning protocol and automatic retinal blood vessel segmentation algorithm. All experiments described here were approved by the University of Waterloo Animal Research Ethics Committee and adhered to the ARVO Statement for Use of Animals in Ophthalmic and Vision Research. The rats were anesthetized with ketamine/xylazine (0.2 ml/100 g body weight) delivered intraperitoneally, and a subcutaneous injection of 5-ml sterile saline was administered immediately after to keep the animal well hydrated during the imaging procedure. The rat's head was stabilized stereotactically and one drop of 0.5% tropicamide (pupillary dilator; Alcon) was applied to each eye. One drop of 0.5% proparacaine hydrochloride (topical anaesthetic; Alcaine, Alcon) was applied to the imaged eye, and artificial tears were administered every 5 min to keep the cornea well hydrated and optically transparent.

A flow chart of the proposed new approach to evaluation of the absolute and pulsatile retinal BF is shown in Fig. 1. A doughnut-shaped area of the rat retina, centered at the ONH was imaged using a dense concentric circular scan pattern [Fig. 1(a)]. Two-hundred concentric circular scans with diameters ranging from 0.8 to 1 mm were used to cover the imaged retinal area. Each concentric scan was comprised of 3000 A-scans, which offered overlap between adjacent A-scans of 78% to 84%, dependent on the diameter of the circular scan. The camera acquisition rate was set to 47 kHz resulting in a frame rate of 15.7 fps

and total acquisition time of 12.7 s. To calculate the absolute BF for each retinal blood vessel, the information from each complex OCT image was divided into two parts: the amplitude was used to segment the retinal blood vessels [Figs. 1(b)–1(d)] while the phase was used to calculate the axial BF [Fig. 1(e)]. A three-step method was used to segment the retinal blood vessels. First, the retinal surface was segmented automatically in each circular DOCT scan [Fig. 1(b)]. Second, a shadow diagram was generated for each circular DOCT scan by averaging the intensity of the OCT image between inner plexiform /outer plexiform boundary and the retinal pigmented epithelium. Then, an *en-face* shadow image was composed by combining all 200 axial OCT shadow diagrams. The dark areas in the *en-face* shadow image [Fig. 1(c)] correspond to the retinal blood vessels. Third, an algorithm based on modified graph theory and a dynamic programming[19] was developed and used to segment automatically the retinal blood vessels from the *en-face* shadow image. The two boundaries for each blood vessel were segmented pair-wisely and different blood vessels were segmented in sequence. Note that for branching blood vessels, only one branch was segmented by the automatic algorithm, while the second branch was ignored [yellow arrow in Fig. 1(c)].

Once the vessels' segmentation was complete, a retinal surface elevation map was generated with all the segmented blood vessels labeled on it [Fig. 1(d)]. The axial and lateral displacements of each blood vessel along radial direction were determined from the surface elevation map and the Doppler angle was calculated using
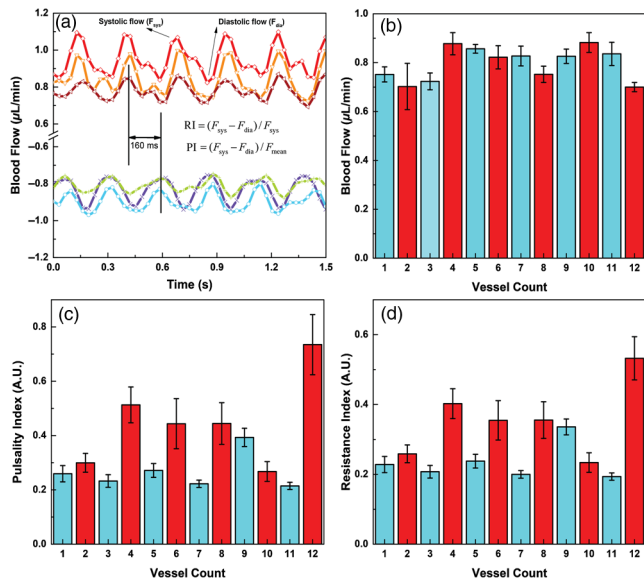
$$\theta = \arccos\left(\frac{\Delta z}{\sqrt{\Delta x^2 + \Delta y^2 + \Delta z^2}}\right).$$

Here, Δy and Δz are the lateral and axial displacements of the blood vessel between adjacent circular scans, respectively, and Δx is the distance between adjacent circular scans (0.5 μm). The absolute retinal BF for the i'th concentric circular DOCT scan was calculated by dividing the axial BF by the corresponding Doppler angle [formula in Fig. 1(g)]. In this study, Doppler angles larger than 85 deg were excluded from the data analysis, as the imprecision of calculating the absolute retinal BF is strongly dependent on $1/\cos(\theta)$.[6]
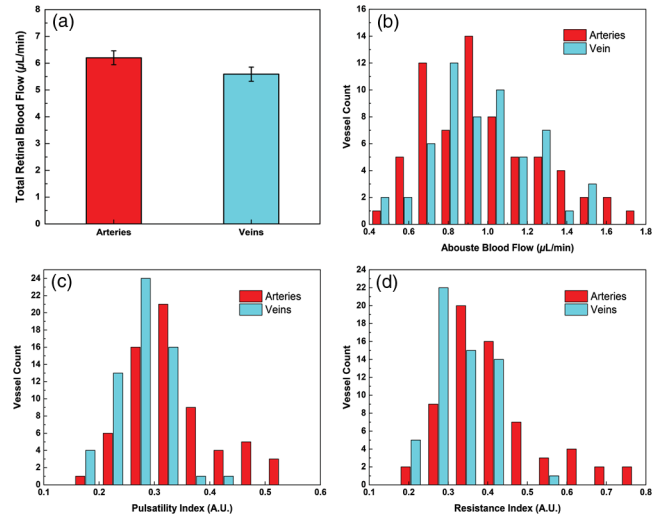
3 Results and Discussion

Representative time traces of the retinal BF measured from three arteries and three veins in one rat are shown in Fig. 2(a). These traces were selected to show the minimum, maximum, and mean BF pulsatility magnitude for all the retinal vessels of that animal. A 1.5-s time window shows five complete cardiac cycles and an average arteriovenous delay of 160 ms that was determined by applying a cross correlation method[20] to the sum of the arterial and venous flow. Quantitative metrics of the pulsatile BF, such as the mean BF, the pulsatility index (PI), and the resistance index (RI), were used to analyze the pulsatile BF. For each retinal blood vessel, the mean BF was calculated by averaging the BF within the time window, while the PI and RI were calculated using the definition formulas shown in Fig. 2(a). To test the reproducibility of the pulsatile BF data, the same scanning protocol was repeated ($n = 6$) in the same animal with 3-min time interval between consecutive measurements. Statistical data for the BF, PI, and RI are shown in Figs. 2(b)–2(d), where arteries are marked in red color and veins in blue color. Although the absolute magnitudes for the arterial and venous BF were very similar and ranged from ∼0.7 to ∼0.9 μL/ min, the arterial PI and RI values were higher than the ones determined for retinal veins, which is as expected.

The same scanning protocol was applied to nine additional animals and the statistical results are shown in Fig. 3 and Table 1. The average total retinal BF was 6.2 ± 0.8 μL/ min in arteries and 5.6 ± 0.8 μL/ min in veins. The difference between the arterial and venous total BF is most likely due to failure of the automatic segmentation algorithm to recognize and account for some of the retinal veins, as the veins in the shadow images may be of too low contrast to be segmented automatically with high confidence. Specifically in all 10 animals, the segmentation algorithm successfully identified and segmented a total of 66 arteries and only 56 veins. Figure 3(b) shows a histogram of the absolute BF measured from all segmented blood vessels. Arterial flow showed a slightly broader distribution compared
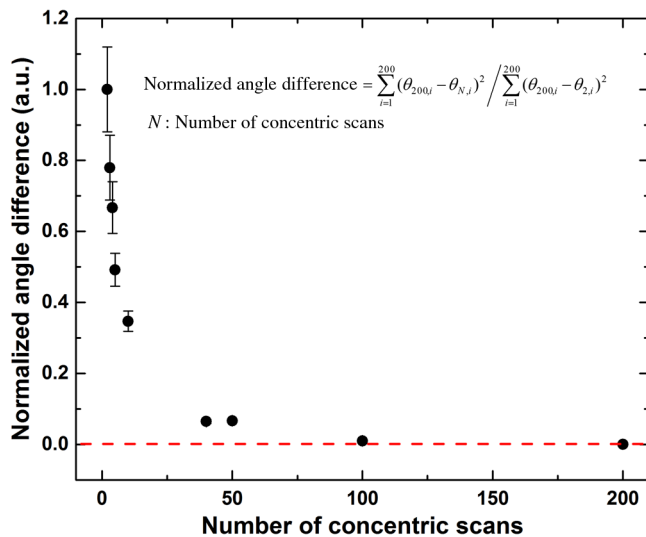

Fig. 3 (a) Statistical results for the total RBF measured from all animals in the study ($n = 10$). (b–d) Histograms show the number of retinal vessels as functions of the mean RBF, PI, and RI.

Table 1 Statistical results for the pulsatile BF metrics obtained from 10 animals.

	Minimum	Maximum	Median	Coefficient of variation
Arterial flow	0.48	1.74	0.94	0.29
Venal flow	0.50	1.54	0.92	0.25
RI (arteries)	0.18	0.73	0.38	0.30
RI (veins)	0.17	0.56	0.31	0.20
PI (arteries)	0.17	0.53	0.32	0.24
PI (veins)	0.16	0.27	0.44	0.18

to venous flow; however, the centroids for arterial venous BF histograms were almost identical. Furthermore, the mean absolute BF per vessel was very similar: 0.93 ± 0.28 μL/ min in arteries versus 0.98 ± 0.26 μL/ min in veins. Figures 3(c) and 3(d) show histograms for the PI and RI, respectively, determined from all segmented blood vessels. The average PI for all the retinal arteries was 22% higher than the average PI measured for all retinal veins. Similarly, the average RI for all the retinal arteries was 28% higher than the RI measured in all the retinal veins.

To evaluate the performance of the proposed new method for accurate assessment of pulsatile BF, results from the dense concentric circle protocol were compared with results from the dual-concentric circle protocol[6] using the same raw data. For the dual-circle protocol, the innermost and outermost of the 200 concentric scans were used to calculate the Doppler angle, while the eight central circular scans that covered one full cardiac cycle were used to calculate the mean axial BF. Results showed 3.8 ± 2.2 deg difference in the Doppler angle assessment between the dense concentric circle and the dual-concentric circle protocols, which resulted in ∼7% difference in the assessment of the absolute BF. Considering the fact that the dual-concentric circle scanning protocol does not account for changes in the spatial orientation of blood vessels with respect to the

Fig. 2 (a) Representative pulsatile BF recordings acquired from three arteries and three veins of one rat. The averaged arteriovenous delay was measured to be 160 ms. (b–d). The mean retinal BF, PI, and RI calculated from 12 segmented retinal blood vessels in one rat (red, arteries; blue, veins). Data are presented as mean ± S.E.

Fig. 4 Precision of the measured Doppler angle as a function of the number of concentric circular scans.

incident direction of the OCT imaging beam, it is natural to conclude that the dense concentric circle scanning protocol allows for more accurate assessment of the Doppler angle and consequently, the absolute retinal BF.

In the animal experiments described here, the combination of anesthesia and head restriction with a custom stereotaxic stage reduced the head and eye motion significantly. This allowed us to explore a scanning protocol with a higher number of concentric circles to map more precisely the spatially varying Doppler angle. In contrast, the eye motion in human subjects is more pronounced and the retinal BF is faster, therefore applying this approach to human clinical studies will require setting the camera A-line rate to 92 kHz and reducing the number of concentric circular scans, in order to shorten the image acquisition time and minimize eye motion-related artifacts. We investigated how reduction in the number of concentric circles will affect the precision of measuring the spatially varying Doppler angle and the relevant data are summarized in Fig. 4. From this analysis, it is clear that using 40 concentric circles can provide a fairly precise evaluation of the spatially dependent Doppler angle. Combined with an increase of the camera A-line rate to 92 kHz, this can shorten the image acquisition time for the procedure to <1.5 s. Although the human eye is much larger than the rat eye and the diameter of the concentric circles would increase proportionally, the fact that the human eye has a significantly smaller NA than the rat eye will reduce the lateral OCT resolution in the human eye by ~3× to 4× compared to the rat eye. Therefore, a scanning protocol of 3000 A-scans per concentric circle will result in sufficient overlap between neighboring A-scans, necessary to generate a DOCT signal of good quality. By reducing the image acquisition time to ~1.5 s in humans, the effect of eye motion on the quality of the DOCT data will be reduced significantly. Different motion correction algorithms can also be applied to further minimize the effect of any residual eye motion-related artifacts.

In conclusion, a dense concentric circle scanning protocol was developed using a camera with a relatively slow image acquisition rate (47 kHz) to measure accurately the pulsatile BF in retinal arteries and veins of the rat retina with SD-OCT. This method offers simplicity of the OCT system design, scanning protocol, and data analysis, as well as better accuracy

in the measurement of the Doppler angle and the assessment of the pulsatile retinal BF. Although this method was tested in the animal retina, it can be easily adapted to imaging and assessment of retinal BF in the human eye by using the full speed of the camera (92 kHz). Because of its simplicity and accuracy, this method can find applications in both clinical studies and fundamental animal research of potentially blinding retinal diseases.

Disclosures

The authors have no relevant financial interests in this article and no potential conflicts of interest to disclose.

References

1. V. Patel et al., "Retinal blood flow in diabetic retinopathy," *BMJ* **305**(6855), 678–683 (1992).
2. W. H. Morgan et al., "Retinal venous pulsation: expanding our understanding and use of this enigmatic phenomenon," *Prog. Retinal Eye Res.* **55**, 82–107 (2016).
3. E. Sato et al., "Retinal haemodynamics in patients with age-related macular degeneration," *Eye* **20**(6), 697–702 (2006).
4. J. Flammer et al., "The impact of ocular blood flow in glaucoma," *Prog. Retinal Eye Res.* **21**(4), 359–393 (2002).
5. J. Yi et al., "Visible light optical coherence tomography measures retinal oxygen metabolic response to systemic oxygenation," *Light Sci. Appl.* **4**(9), e334 (2015).
6. T. Nagaoka et al., "Evaluation of retinal circulation using segmental-scanning Doppler optical coherence tomography in anesthetized cats," *Invest. Ophthalmol. Visual Sci.* **57**(7), 2936–2941 (2016).
7. M. D. Knudtson et al., "Variation associated with measurement of retinal vessel diameters at different points in the pulse cycle," *Br. J. Ophthalmol.* **88**(1), 57–61 (2003).
8. R. A. Leitgeb et al., "Doppler optical coherence tomography," *Prog. Retinal Eye Res.* **41**, 26–43 (2014).
9. L. M. Peterson et al., "Orientation-independent rapid pulsatile flow measurement using dual-angle Doppler OCT," *Biomed. Opt. Express* **5**(2), 499–514 (2014).
10. C. Blatter et al., "Dove prism based rotating dual beam bidirectional Doppler OCT," *Biomed. Opt. Express* **4**(7), 1188 (2013).
11. A. S. G. Singh et al., "Stable absolute flow estimation with Doppler OCT based on virtual circumpapillary scans," *Biomed. Opt. Express* **1**(4), 1047–1058 (2010).
12. S. Huang et al., "In vivo imaging of retinal hemodynamics with OCT angiography and Doppler OCT," *Biomed. Opt. Express* **7**(2), 663 (2016).
13. B. K. Lee et al., "Cardiac-gated en face Doppler measurement of retinal blood flow using swept-source optical coherence tomography at 100,000 axial scans per second," *Invest. Ophthalmol. Visual Sci.* **56**(4), 2522–2530 (2015).
14. O. Tan et al., "En face Doppler total retinal blood flow measurement with 70 kHz spectral optical coherence tomography," *J. Biomed. Opt.* **20**(6), 066004 (2015).
15. B. Tan et al., "Correlation of visually evoked functional and blood flow changes in the rat retina measured with a combined OCT+ERG system," *Invest. Opthalmol. Visual Sci.* **58**(3), 1673 (2017).
16. S. Hariri et al., "Noninvasive imaging of the early effect of sodium iodate toxicity in a rat model of outer retina degeneration with spectral domain optical coherence tomography," *J. Biomed. Opt.* **18**(2), 026017 (2013).
17. A. A. Moayed et al., "In vivo imaging of intrinsic optical signals in chicken retina with functional optical coherence tomography," *Opt. Lett.* **36**(23), 4575 (2011).
18. A. Standard, "American national standard for the safe use of lasers," Z136.1 2007–1, American National Standards Institute, Inc., New York (2007).
19. F. Larocca et al., "Robust automatic segmentation of corneal layer boundaries in SDOCT images using graph theory and dynamic programming," *Biomed. Opt. Express* **2**(6), 1524–1538 (2011).
20. F. Moret et al., "Quantitative analysis of fundus-image sequences reveals phase of spontaneous venous pulsations," *Transl. Visual Sci. Technol.* **4**(5), 3 (2015).